J Appl Phycol (2017) 29:1851–1863
DOI 10.1007/s10811-017-1071-0

Comparative studies of three novel freshwater microalgae strains for synthesis of silver nanoparticles: insights of characterization, antibacterial, cytotoxicity and antiviral activities

Muneeba Khalid[1] · Nauman Khalid[2,3] · Iftikhar Ahmed[4] · Rumeza Hanif[1] · Muhammad Ismail[5] · Hussnain Ahmed Janjua[1]

Received: 19 August 2016 / Revised and accepted: 23 January 2017 / Published online: 9 March 2017

Abstract The therapeutic efficacy of universal drug-delivery systems depends on their capability to escape the immune system by overcoming the biological barriers of the body and concentrate at target tissues to eradicate only diseased cells. Biologically synthesized nanoparticle systems possess almost all of these qualities and utilize their targeting ability through cellular membrane interactions and making the targeting system biocompatible. In the present study, microalgae-mediated silver nanoparticles (AgNPs) targeted bacterial, fungal, cancerous and viral infected cells without harming normal cells. These AgNPs provide a comparative study on broader range of size and shape, synthesized by ethanolic extract of three different freshwater microalgae species, *Dictyosphaerium* sp. strain HM1 (DHM1), *Dictyosphaerium* sp. strain HM2 (DHM2) and *Pectinodesmus* sp. strain HM3 (PHM3). Characterization of AgNPs was done by XRD, SEM, TEM, EDS, FTIR and UV-Vis spectrophotometry. Significant activity against 14 bacterial strains, the fungal strain *Candida albicans*, hepatocellular carcinoma (HepG2) and breast cancer (MCF7) cell lines, and Newcastle Disease Virus (NDV) on Huh7-infected cells suggest the potential use of microalgae extract prepared nanoparticles in biomedicine, pharmaceutics and drug delivery.

Keywords Silver nanoparticles · Microalgae extract · Biocompatible · Hepatocellular carcinoma · Breast cancer · Newcastle disease virus

Introduction

Biological methods using plants, algae, fungi and bacteria for synthesis of metallic nanoparticles have potential to alter the landscape of biomedicine (Gurunathan et al. 2009; Jena et al. 2013; Nayak et al. 2011). They provide size- and shape-dependent properties for nanoparticle (NP) synthesis in a sustainable aseptic environment (Durán et al. 2010). Amongst these biological systems, algae synthesize a range of nutraceuticals such as lipids, minerals, vitamins, polysaccharides and proteins (El Baky and El-Baroty 2013; Joana Gil-Chávez et al. 2013). These algal bioactive compounds show remarkable medicinal activities with potential to be used to cure cancer, inflammation, oxidative stress and other degenerative diseases (Nishino et al. 1999; Mohamed et al. 2012). The presence of capping and reducing agents in algal extracts (hydroxyl, carboxyl and amino functional groups) ensures coating of metallic nanoparticles for functional superstructures (Namvar et al. 2012; Mahdavi et al. 2013). Amongst the metallic NPs, silver nanoparticles (AgNPs) are used

Electronic supplementary material The online version of this article (doi:10.1007/s10811-017-1071-0) contains supplementary material, which is available to authorized users.

✉ Hussnain Ahmed Janjua
hussnain.janjua@asab.nust.edu.pk; janjua.hussnain@gmail.com

[1] Department of Industrial Biotechnology, Atta-ur-Rahman School of Applied Biosciences, National University of Science and Technology (NUST), Islamabad, Pakistan

[2] School of Food and Agricultural Sciences, University of Management and Technology, Lahore 54000, Pakistan

[3] Centre for Chemistry and Biotechnology, School of Life and Environmental Sciences, Deakin University, Waurn Ponds, Victoria 3216, Australia

[4] Institute of Microbial Culture Collection of Pakistan (IMCCP), National Agricultural Research Centre (NARC), Park Road, Islamabad 45500, Pakistan

[5] Institute of Biomedical and Genetic Engineering (IBGE), 24 Mauve Area, Sector G-9/1, Islamabad, Pakistan

extensively in catalysis, biomedical applications, electronics and sensors (Abbasi et al. 2016; Ihsan et al. 2015). As a therapeutic, AgNPs have shown antimicrobial, antifungal, anticancer, antiviral, anti-inflammatory, anti-angiogenesis and antiplatelet activities (Namasivayam et al. 2015). Various nano-Ag products, comprising contraceptive devices, surgical instruments, implants, AgNP-coated wound dressings detergents, wall paints and textile industry cloth manufacturing chemicals are commercially available (Gottesman et al. 2010; Feng et al. 2011; Martínez-Gutierrez et al. 2012; You et al. 2012).

A number of algae species from the Chlorophyta (e.g., *Pithophora oedogonia*, *Caulerpa racemosa*, *Chlorella vulgaris*), Phaeophyta (e.g., *Sargassum wightii*, *Padina tetrastromatica*, *Turbinaria ornata*) and Rhodophyta (e.g., *Gracilaria edulis*) extracts have been used to synthesize AgNPs (Patel et al. 2015; Satapathy et al. 2015; Sunitha et al. 2015; Sharma et al. 2016). Biologically synthesized AgNPs in above mentioned algae species were therapeutically tested, especially for antibacterial activity. Other therapeutic activities are still underexplored, whereas these studies provided evidence that algae-mediated AgNPs can be used for controlled and targeted drug delivery. Previously studied microalgae-mediated nano-products strictly followed similar activity pattern for only bacteria with very narrow size and shape range, usually below 20 nm (Patel et al. 2015). The toxic activity of biologically synthesized AgNPs is little reported for fungal cells and/or viral cells (Mukherjee et al. 2001).

In the present study, three different freshwater microalgae strains were used to synthesize AgNPs using their ethanolic extracts and the ability of these nanoparticles to inhibit bacterial, fungal and viral infections as well as cancer cells was verified. Infectious diseases during treatment in hospitals are reported frequently and not only increase cost and duration of hospitalization but also patient morbidity (Mermel et al. 2009). Fungemia and bacteremia are the two most commonly observed infectious diseases during clinical treatments. Fungemia tends to occur in both critical and non-critical ill patients with highest rate of morbidity and/or mortality. *Candida albicans* is one of the major species that are responsible for clinically induced fungemia (Marcos-Zambrano et al. 2014). Patients with bloodstream infections, caused by antibiotic-resistant bacteria of mutant type Enterobacteriaceae, *Pseudomonas aeruginosa* and *Acinetobacter* species are an issue leading to extended hospitalization and/or death due to inadequate treatment and cure of these resilient microorganisms. Besides finding treatment for bacteremia and fungemia, finding anticancer drugs target only tumour cells without excessive toxicity has remained a challenge for decades. These concerns led us to study extracts of microalgae conjugated with metallic NPs to counter these diseases as an alternative for chemically synthesized drugs.

Material and methods

Identification of microalgae strains and media

Fresh water photosynthetic microalgae samples were collected from KallarKahar Lake located at KallarKahar Tehsil (District Chakwal, Punjab, Pakistan). Strains were cultivated in bold basal media (BBM) (Stein 1979) supplied by Phyto Technology Laboratories, Australia. Streaking of fresh water microalgae samples was performed on agar slants and plates to isolate different species from sampled consortium of collected microalgae. Single colonies were picked and subcultured in liquid BBM. Flasks with microalgal inoculum were illuminated with a white fluorescent lamp at 100 μmol photons m^{-2} s^{-1} with a 24-h light cycle. Aeration was provided by aquarium air pumps and culture temperature was maintained at 26–28 °C. Every 14 days, microalgae were harvested and dried for further experiments.

Molecular identification based on sequencing of internal transcribed spacer regions

DNA extraction of microalgae was by the CTAB method (Rogers and Bendich 1994), with some modifications. Microalgae (0.5 g) was ground in a mortar and pestle using liquid nitrogen and 1 μL of polyvinyl pyrrolidone (Haaf et al. 1985). DNA was purified using ethanol precipitation and quantified on a Nanodrop spectrophotometer (Thermo Scientific, UK). Amplification of internal transcribed spacer (ITS) regions and DNA sequencing of the amplicons were performed by Macrogen Inc. Seoul, South Korea (www.dna.macrogen.com). The strains were identified by analysing ITS sequences on the NCBI server using BLAST search. The sequence data of closely related strains used for construction of phylogenetic tree were retrieved from the NCBI database. The alignment and editing was performed using CLUSTAL X (1.8 msw) (Thompson et al. 1997) and BioEdit (Hall 1999) software packages. Ambiguous positions and gaps were excluded during calculations. The phylogenetic trees were constructed by neighbour joining methods using MEGA (Version 6.1) software (Tamura et al. 2013). The stability of the relationship was assessed with bootstrap analysis (Felsenstein 1985), by performing 1000 resampling for the tree topology. Later sequences of all the stains were submitted to DNA Data Bank of Japan (DDBJ).

Preparation of ethanolic microalgae extract

Microalgae were harvested and dried for 3 days at ambient temperature (26–28 °C). Dried microalgae were crushed into powder. Dried powder (1 g) was extracted with 100 mL of HPLC grade ethanol. The microalgae solutions were placed

on a hotplate (VELP Scientific, Italy) for maceration at 78 °C with a magnetic stirrer for 20 min. The solutions were then allowed to cool at room temperature and filtered through 0.2-μm pore size filter and stored at 4 °C.

Biological synthesis of silver nanoparticles

A 5 mM aqueous solution of silver nitrate ($AgNO_3$) (Riedel de Haen, Germany) was prepared and added to ethanolic extracts of microalgae in a ratio of 5:1. The $AgNO_3$ solution and algal extracts were incubated at 37 °C. The ethanolic extract of algae acted as reducing and capping agent for Ag ions in $AgNO_3$ solution.

Surface plasmon resonance spectroscopy (UV-Vis)

Preliminary confirmation of synthesis was the colour change from dark green to brownish yellow after overnight incubation. Synthesized AgNPs were confirmed by observing their kinetic behaviour via UV-visible spectroscopy on a UVD-2950 spectrophotometer. Scanning range of samples was between 300 and 700 nm with a sampling interval of 1 nm. UV-Vis spectra for ethanolic extracts and diluted aliquots of AgNPs were analysed for reducing activity of Ag ions. Absorbance peaks with matching wavelength was observed as a consequence of reduction of metal ions to nanoparticles.

Determination of concentration of the silver nanoparticles

Calculations for determination of AgNP concentration were carried out using the mathematical model of Liu et al. (2007). Firstly, the average number of atoms per nanoparticle was determined using Eq. 1 and later molar concentration was determined using Eq. 2.

$$N = \frac{\pi \rho D^3}{6M} N_A \tag{1}$$

where N is number of Ag atoms per nanoparticle, ρ is density of Ag, D is average size of nanoparticles, M is the Ag atomic weight and N_A is the number of atoms per mole:

$$C = \frac{N_T}{\mathrm{NV}N_A} \tag{2}$$

C is the molar concentration of nanoparticle solution, N_T is the total number of Ag atoms added in $AgNO_3$, N is number of atoms per nanoparticle calculated from Eq. 1 and V is volume of reaction solution (per batch), and N_A is the number of nanoparticles per mole.

Purification of synthesized silver nanoparticles

Synthesized AgNPs were purified by two methods. Primarily, nanoparticles were centrifuged at 1792×g for 60 min; the clear supernatant was discarded and the particles were washed three times with deionized water. After centrifugation, the concentrated solution of AgNPs was purified by dialysis with deionized water. A 3-day protocol was followed for AgNPs by changing water and washing membrane every 24 h. The concentrated solutions of AgNPs were lyophilized, to obtain a dry powder of AgNPs. The procedure yielded 2–3 g per 500 mL solution.

Scanning electron and transmission election microscopies

SEM was performed using analytical low vacuum scanning electron microscope (JEOL, JSM-6490LA, Japan) at 20 kV. A 10-μL aliquot of AgNPs was suspended in 1 mL of deionized water. Diluted colloidal solutions of AgNPs were sonicated in a glass beaker for 1 h. One drop from each beaker was placed on a 1-cm^2 glass slide and dried under a UV-lamp. The samples were sputter coated with gold before SEM examination.

The size and shape of the synthesized AgNPs were determined by TEM. The TEM images of synthesized AgNPs were obtained using a JEOL (Model JEM-1010, Japan) TEM. Prior to analysis, AgNPs were sonicated for 5 min, and a drop of appropriately diluted sample was placed onto a carbon-coated copper grid. The liquid fraction was allowed to evaporate at room temperature.

Fourier transform infrared spectroscopy

FTIR of the sample was performed on Perkin-Elmer Spectrum-100 FTIR. Scanning range for samples was set in region 450–4000 cm^{-1} with a resolution of 1 cm^{-1}. Potassium bromide (KBr) pellet, AgNPs and ethanolic extract were made using hydraulic press with 1 μg of respective powder and KBr. Essential FTIR (eFTIR; v3.10.041) software was used to confirm peaks followed by results description.

X-ray diffraction

The XRD pattern was recorded with a STOE Theta-Theta X-ray diffractometer Germany, furnished with copper K alpha radiation source, operating voltage of 40 kV and functional current of 40 mA. Samples were prepared on 1-cm^2 slides by suspending lyophilized powder in 0.5 mL of deionized water.

Energy dispersive X-ray spectroscopy

Presence of different phases in sample was revealed by EDS attached to SEM. Accelerating voltage of machine was sustained at 20 kV with probe current of 1 mA. PHA mode T_3 with real time of 56.03 s and live time of 50 s for analyser. Counting rate was 2785 for AgNPs and energy range was 0–20 keV. Samples were mounted in the form of dried lyophilized powder on a slide of 1 cm^2, sputter coated with gold prior mounting.

Evaluation of antibacterial and antifungal activity and disc diffusion assay

Mueller Hington Agar (MHA) cultures of test microorganisms using standardized inocula of bacterial and fungal strains (Ishtiaq et al. 2013) at a cell density of 1×10^8 cells mL^{-1}. Disc diffusion assay was performed for analysing bactericidal activity (Karcioglu et al. 2011). The strains were streaked on agar plates and 6-mm discs impregnated with AgNPs (10 μL) were used. Positive controls of standard antibiotics cefepime (FEP) 100 μg mL^{-1}, tigecycline (TGC) 100 μg mL^{-1} and negative control of simple solvent-permeated discs were used. In addition, ethanolic extracts of the respective microalgae were also checked against bacterial strains. The plates were incubated at 37 °C for 24 h and zones of inhibition were measured.

Cytotoxicity of silver nanoparticles

Human hepatocellular carcinoma (hepG2), breast cancer (MCF7) and Huh7 cell lines were provided by the Institute of Biotechnology and Genetic Engineering (IBGE), Islamabad, Pakistan. Cell lines were maintained in RPMI media (Freshney 2005) with 10% foetal bovine serum (FBS) and 1% antibiotic-antimycotic solution. Cells were grown at 37 °C and 5% CO_2 in CO_2 incubator (SL Shell Lab, Germany) and seeded onto the plates after sustaining density of 1×10^6 cells $(100\ \mu L)^{-1}$ in a single well.

Five different concentrations of AgNPs were prepared by dissolving 10–50 μg of lyophilized AgNPs per 1 mL of autoclaved distilled water. Appropriate amount of each concentration was added to culture cells followed by incubation of plates at 37 °C for 24 h in CO_2 incubator. A column of wells with non-treated cells were taken as control and time activity was observed. Human corneal epithelial cells (HCECs) were used for evaluation of biocompatibility of AgNPs. After 24 h of incubation, cells with AgNPs 10 μL MTT (3-(4,5-dimethylthiazol-2-yl)-2,5-diphenyltetrazolium bromide, a tetrazole) were added and incubated at 37 °C for another 24 h. Absorbance at 550 nm was measured on a microplate ELIZA plate reader (Platoz R 496, Egypt). The data obtained was standardized by determining the absorbance, and a plot for dose-response curve was plotted for IC_{50} value assessment as follows:

$$\text{Cell viability in}\% = (\text{Mean OD}_{550}/\text{control OD}_{550}) \times 100 \quad (3)$$

$$\%\text{inhibition} = 100 - \text{Cell viability in}\ \% \quad (4)$$

where OD is the optical density value obtained from the spectrophotometer. DNA of AgNP-treated cell lines was extracted using phenol/chloroform method (Chomczynski and Sacchi 1987) with some modifications. The extracted DNA was visualized on a 1.5% agarose gel by gel electrophoresis and quantified using a Nanodrop spectrophotometer.

Antiviral assay and antiviral activity of silver nanoparticles

Newcastle disease virus (NDV) was from the Mukhteshwar strain (supplied by Punjab Poultry Institute, Rawalpindi, Pakistan) and inoculated in 8-day-old embryonated eggs. The eggs were incubated at 37 °C for 24 h and amniotic fluid was taken as virus titre. Hemagglutination (HA) test was performed on 96-well plates with 50 μL of PBS, 50 μL virus titre and 50 μL of 5% chicken blood (washed with PBS) at 37 °C for about 30 min. Non-agglutinated red blood cells at the base of control wells were indication of completion of test. Wells with virus showed agglutination and remained suspended and appeared as pinkish red solution; however, wells without virus formed a clump and appeared as button at the end of round-bottom wells.

$TCID_{50}$ value was calculated using the method of Pizzi (1950) with some modifications. Huh7 cells were plated on 96-well plates and left for 24 h in incubator at 37 °C provided with 5% CO_2. After 24 h, the medium was removed and 50 μL of virus dissolved in PBS with different concentrations (10^{-1} up to 10^{-7}) was added. Plates were incubated for 2 h followed by medium replacement by RPMI with 2% FBS. The plate was incubated and observed every day under inverted microscope for plaque formation. At day 3, NDV showed plaque formation. $TCID_{50}$ dose for antiviral activity was calculated by taking readings of wells containing infected cells with virus.

Huh7 cells (100 μL) were plated in each well of 96-well plate, infected by 50 μL of virus and incubated for 2 h. The medium was removed and replaced with RPMI and 2% FBS. Further proceedings included addition of AgNPs of different concentration and incubation at 37 °C in a CO_2 incubator. The plate was observed after every 24 h until control cells showed viral growth. MTT was added and plates were incubated for further 4 h. Reading in an ELIZA plate reader was taken after addition of solubilization solution.

Results

Identification of microalgae

PCR amplification of ITS region and sequence analysis using BLAST search revealed that two strains of microalgae belonged to the genus, *Dictyosphaerium*, while a third strain was closely related to the genus, *Pectinodesmus*. The results of phylogenetic analysis showed that strains DHM1 and DHM2 clustered with three undefined strains of *Dictyosphaerium* (Fig. 1a), having sequence similarities of 97.9 and 95.6%, respectively. The cluster comprising of these two strains together with three undefined closely related strains of *Dictyosphaerium* form a separate clade, which is distant to other clusters of known species. The results suggest that this clade comprising of our strains DHM1 (LC159305) and DHM2 (LC159306) together with three undefined strains could be a new species in the genus *Dictyosphaerium*. However, further taxonomic studies will be needed to delineate a new species, which is beyond the scope of this manuscript. The sequence analysis showed that the strain PHM3 (LC159307) has 99.3% sequence similarity with *Pectinodesmus pectinatus* (HG514429) and clusters with it at high bootstrap value (82%) (Fig. 1b).

Confirmation and characterization of microalgae-mediated silver nanoparticles

Synthesized AgNPs were confirmed and characterized using UV-Vis, SEM, TEM, FTIR, XRD and EDS to investigate their chemical and physical properties.

Surface plasmon resonance by using UV-Vis spectrophotometry The intense yellowish brown colour was observed for AgNPs and mainly due to surface plasmon resonance (SPR). The size of AgNPs plays a vital role in SPR's red or blue shift. Smaller or quantum size AgNPs tend to possess UV peaks around 400 nm while average to larger sizes increase the SPR wavelength (Asharani et al. 2008). In this study, Ag ions of $AgNO_3$ solution were reduced to AgNPs by shifting with the wavelength of the reaction mixture shifting from dark green to a persistent yellowish brown, when left overnight at 37 °C and pH 7.5. The Ag SPR band for DHM1-AgNPs appeared at 419 nm, while absorption band for DHM2-AgNPs was at 421 nm, and PHM3-AgNPs showed peak at 418 nm (Fig. S1a, b, c).

Scanning electron microscopy SEM showed that the average size (d_{av}) for DHM1-AgNPs was 22.5 nm, 47.5 nm for DHM2-AgNPs and 57.5 nm for PHM3-AgNPs (Fig. S2a, b, c). DHM1-AgNPs and DHM2-AgNPs appeared relatively uniform and spherical, while PHM3-AgNPs were ovoid-shaped AgNPs. SEM images also exhibit agglomerated particles of larger sizes in all synthesized AgNPs. For confirmation of appropriate size of NPs and to avoid imaging of any microalgae residue, ethanolic extracts were filtered and synthesized NPs were purified by dialysis that eliminates the imaging of any other entity.

Transmission electron microscopy TEM confirmed the structure and size distribution of DHM1-AgNPs and DHM2-AgNPs which predominately were spherical in shape with smooth edges (Fig. 2a, b) depicting d_{av} range of 15 to 30 nm and 40 to 50 nm, respectively. However, d_{av} of PHM3-AgNPs varied from 50 to 65 nm. The shape appeared spherical to mostly ovoid for PHM3-AgNPs (Fig. 2c). The detail of possible capping agents in our study was provided by FTIR analysis.

Fourier transmission infrared spectroscopy FTIR analysis for DHM1-AgNPs showed a lost peak of amine at 3413 cm^{-1}, aliphatic amine at 1050 cm^{-1}, aromatic group at 879 cm^{-1} and alkenes at 1640 cm^{-1}. Introduction of primary alcohol at 3444 cm^{-1} and aldehyde at 2851 cm^{-1} was also observed. Results also suggested a peak shift of alkanes from 2955 cm^{-1} to 2920 cm^{-1} and primary amines at 1633 cm^{-1} (Fig. 3a).

DHM2-AgNP analysis (Fig. 3b) illustrated lost amine peak at 3408 cm^{-1}, alkane stretch at 2956 and 2900 cm^{-1}, alkane bend at 1452 cm^{-1}, alkane rock at 1329 cm^{-1}, aliphatic amines at 1089 cm^{-1}, ethers at 1049 cm^{-1} and aromatic C–H at 881 cm^{-1}. Introduction of aliphatic amines at 1025 cm^{-1}, nitro compounds at 1516 cm^{-1} and primary amines at 1629 cm^{-1} was an indication for biosynthesis of AgNPs. Reappearance of alkanes at 2850/2918 cm^{-1} and primary alcohols at 3434 cm^{-1} also supported the process of reduction, capping and stabilization. Moreover, peak shift of alkenes from 1645 to 1629 cm^{-1} was observed.

PHM3-AgNPs presented lost peaks of alkene at 1650 cm^{-1}, ethers at 1049 cm^{-1} and aromatic C–H at 881 cm^{-1}. Introduction of aldehydes at 2849 cm^{-1} and primary amines at 163 3 cm^{-1} suggested the reduction and capping of AgNPs, respectively. Peak shift of primary alcohol from 3402 to 3426 cm^{-1} and alkane from 2976 to 2918 cm^{-1} accompanied by reoccurrence of aliphatic amine at 1018 cm^{-1} was also detected (Fig. 3c).

X-ray diffraction The crystalline structure of the AgNPs was determined by XRD under 2θ full spectrum ranging from 10° to 80°. Four distinct characteristic sharp diffraction peaks of Ag for DHM1-AgNPs were observed at 38.11°, 44.29°, 64.44° and 77.39° (Fig. 4a). These values were assigned the plane (111), (200), (220) and (311) indicated face-centric cubic (fcc) crystals of AgNPs. XRD spectrum for DHM2-AgNPs (Fig. 4b) showed peaks at 38.04°, 47.06° and 54.99° which corresponds to the plane (111), (200) and (220) and represents fcc crystal structure of Ag. On the other hand, 2θ

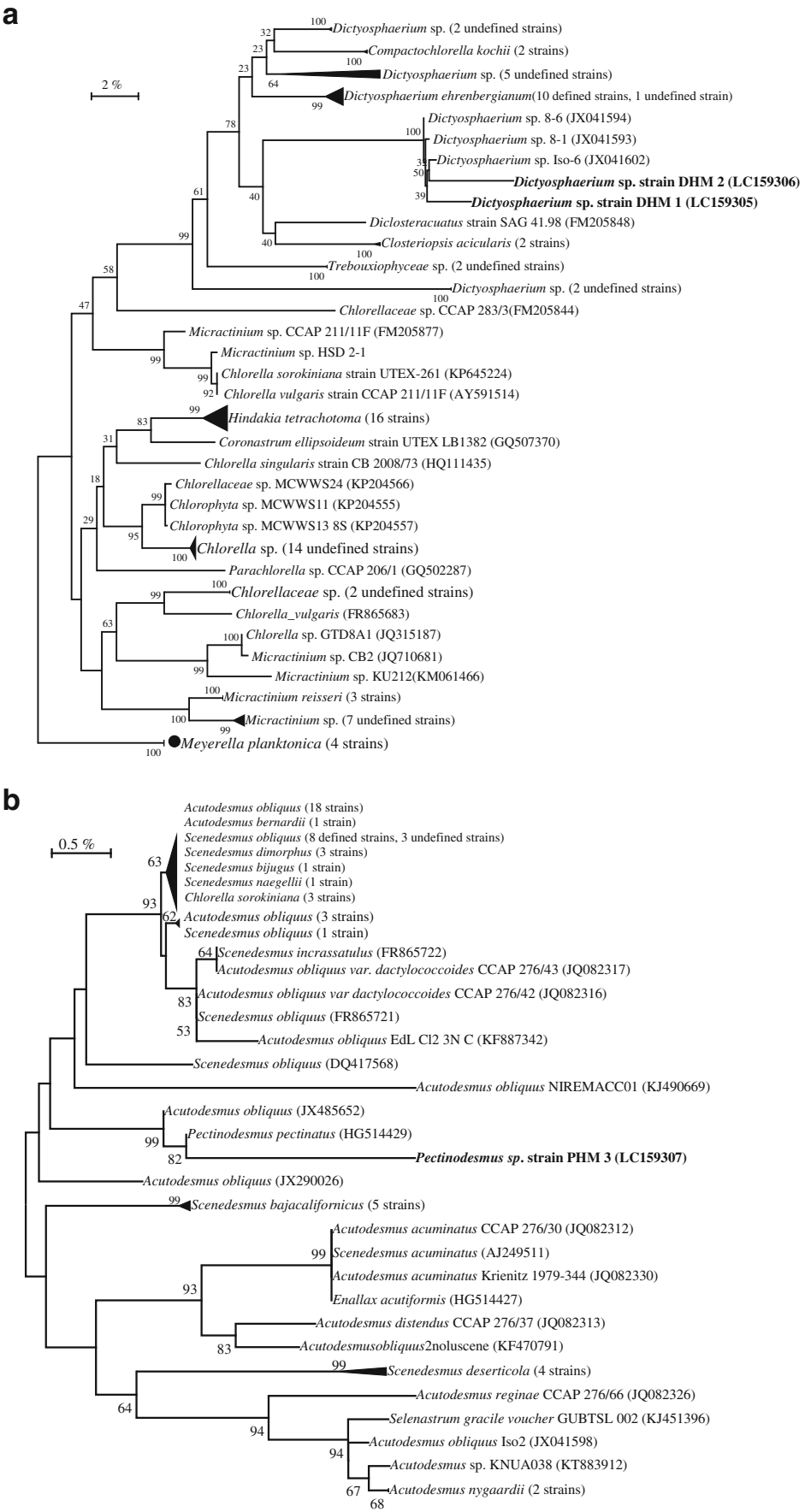
a
2 %
Dictyosphaerium sp. (2 undefined strains)
Compactochlorella kochii (2 strains)
Dictyosphaerium sp. (5 undefined strains)
Dictyosphaerium ehrenbergianum(10 defined strains, 1 undefined strain)
Dictyosphaerium sp. 8-6 (JX041594)
Dictyosphaerium sp. 8-1 (JX041593)
Dictyosphaerium sp. Iso-6 (JX041602)
Dictyosphaerium sp. strain DHM 2 (LC159306)
Dictyosphaerium sp. strain DHM 1 (LC159305)
Diclosteracuatus strain SAG 41.98 (FM205848)
Closteriopsis acicularis (2 strains)
Trebouxiophyceae sp. (2 undefined strains)
Dictyosphaerium sp. (2 undefined strains)
Chlorellaceae sp. CCAP 283/3(FM205844)
Micractinium sp. CCAP 211/11F (FM205877)
Micractinium sp. HSD 2-1
Chlorella sorokiniana strain UTEX-261 (KP645224)
Chlorella vulgaris strain CCAP 211/11F (AY591514)
Hindakia tetrachotoma (16 strains)
Coronastrum ellipsoideum strain UTEX LB1382 (GQ507370)
Chlorella singularis strain CB 2008/73 (HQ111435)
Chlorellaceae sp. MCWWS24 (KP204566)
Chlorophyta sp. MCWWS11 (KP204555)
Chlorophyta sp. MCWWS13 8S (KP204557)
Chlorella sp. (14 undefined strains)
Parachlorella sp. CCAP 206/1 (GQ502287)
Chlorellaceae sp. (2 undefined strains)
Chlorella_vulgaris (FR865683)
Chlorella sp. GTD8A1 (JQ315187)
Micractinium sp. CB2 (JQ710681)
Micractinium sp. KU212(KM061466)
Micractinium reisseri (3 strains)
Micractinium sp. (7 undefined strains)
Meyerella planktonica (4 strains)
b
0.5 %
Acutodesmus obliquus (18 strains)
Acutodesmus bernardii (1 strain)
Scenedesmus obliquus (8 defined strains, 3 undefined strains)
Scenedesmus dimorphus (3 strains)
Scenedesmus bijugus (1 strain)
Scenedesmus naegellii (1 strain)
Chlorella sorokiniana (3 strains)
Acutodesmus obliquus (3 strains)
Scenedesmus obliquus (1 strain)
Scenedesmus incrassatulus (FR865722)
Acutodesmus obliquus var. dactylococcoides CCAP 276/43 (JQ082317)
Acutodesmus obliquus var dactylococcoides CCAP 276/42 (JQ082316)
Scenedesmus obliquus (FR865721)
Acutodesmus obliquus EdL Cl2 3N C (KF887342)
Scenedesmus obliquus (DQ417568)
Acutodesmus obliquus NIREMACC01 (KJ490669)
Acutodesmus obliquus (JX485652)
Pectinodesmus pectinatus (HG514429)
Pectinodesmus sp. strain PHM 3 (LC159307)
Acutodesmus obliquus (JX290026)
Scenedesmus bajacalifornicus (5 strains)
Acutodesmus acuminatus CCAP 276/30 (JQ082312)
Scenedesmus acuminatus (AJ249511)
Acutodesmus acuminatus Krienitz 1979-344 (JQ082330)
Enallax acutiformis (HG514427)
Acutodesmus distendus CCAP 276/37 (JQ082313)
Acutodesmusobliquus2noluscene (KF470791)
Scenedesmus deserticola (4 strains)
Acutodesmus reginae CCAP 276/66 (JQ082326)
Selenastrum gracile voucher GUBTSL 002 (KJ451396)
Acutodesmus obliquus Iso2 (JX041598)
Acutodesmus sp. KNUA038 (KT883912)
Acutodesmus nygaardii (2 strains)

◀ **Fig. 1** **a** Neighbour-joining phylogenetic tree inferred from sequences of internal transcribed spacer (ITS) showing interrelationship of two strains of microalgae (strain DHM 1 and strain DHM 2) with the closely related strains of different genera. Data with gaps and ambiguous nucleotides were removed during alignment for the construction of tree, which was generated using the MEGA 6.0 software package and was rooted by using *Meyerella planktonica* as an out-group. Bootstrap values (only >60% are shown), expressed as a percentage of 1000 replications, are given at the branching points. Bar 2.0% sequence divergence. **b** Neighbour-joining phylogenetic tree inferred from sequences of ITS showing interrelationship of microalgae strain PHM 3 with the closely related strains of different genera. Data with gaps and ambiguous nucleotides were removed during alignment for the construction of tree, which was generated using the MEGA 6.0 software package (Tamura et al. 2013) and was rooted by using *M. planktonica* as an out-group. Bootstrap values (only >60% are shown), expressed as a percentage of 1000 replications, are given at the branching points. Bar 2.0% sequence divergence

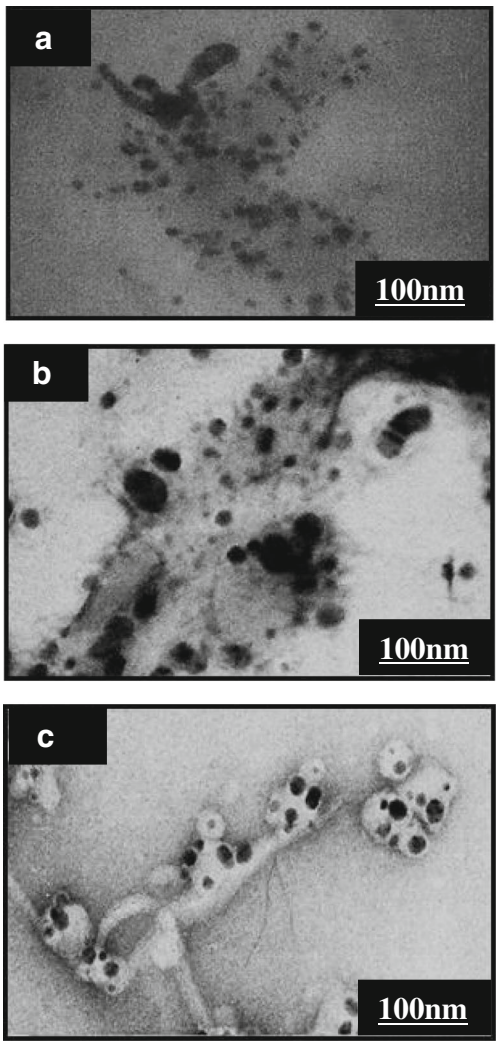

Fig. 2 Transmission electron microscopy images representing morphology of AgNPs **a** DHM1-AgNPs, **b** DHM2-AgNPs and **c** PHM3-AgNPs

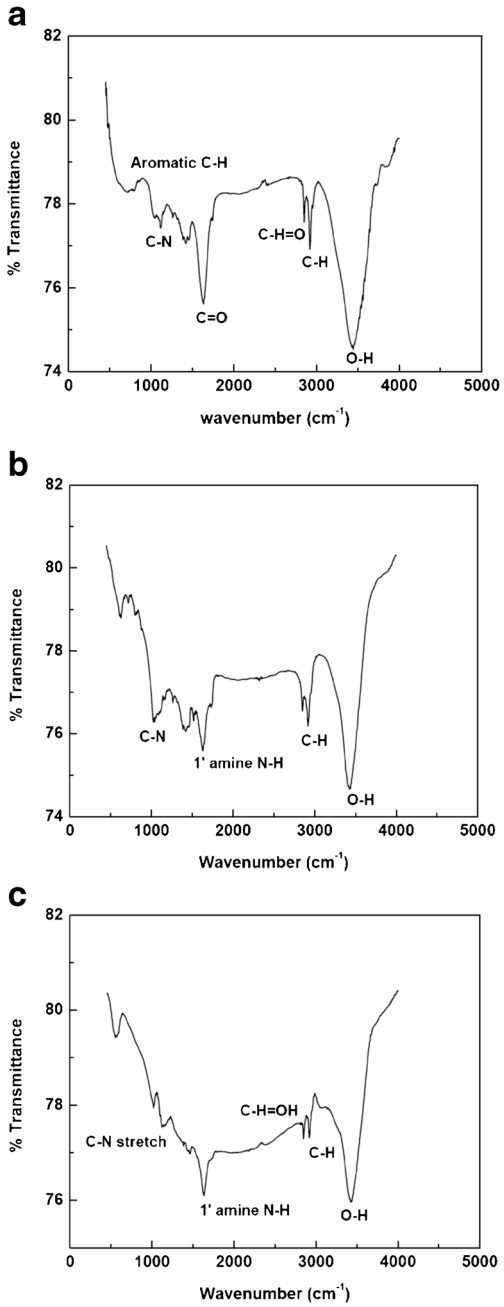

Fig. 3 Fourier transmission infrared spectroscopy presenting peak shifts during AgNPs formation: **a** DHM1-AgNPs, **b** DHM2-AgNPs and **c** PHM3-AgNPs

peak at 32.79° with plane value (110) indicates some quantity of monoclinic NPs of silver oxide (Ag_2O) due to the presence of oxygen and its interaction with Ag. Similarly, for PHM3-AgNPs spectrum, major 2θ peak of monoclinic Ag_2O at 32.8° and a minor peak of Ag at 38.4° allocated planes (110) and (111) were detected (Fig. 4c). The results were also verified by standards of Joint Committee on Powder Diffraction (JCPDS; MDI-Jade 6.5 version). The lattice constant calculated for the pattern was 4.7023 and 4.7605 Å, which is almost consistent with standard value of 4.090 Å.

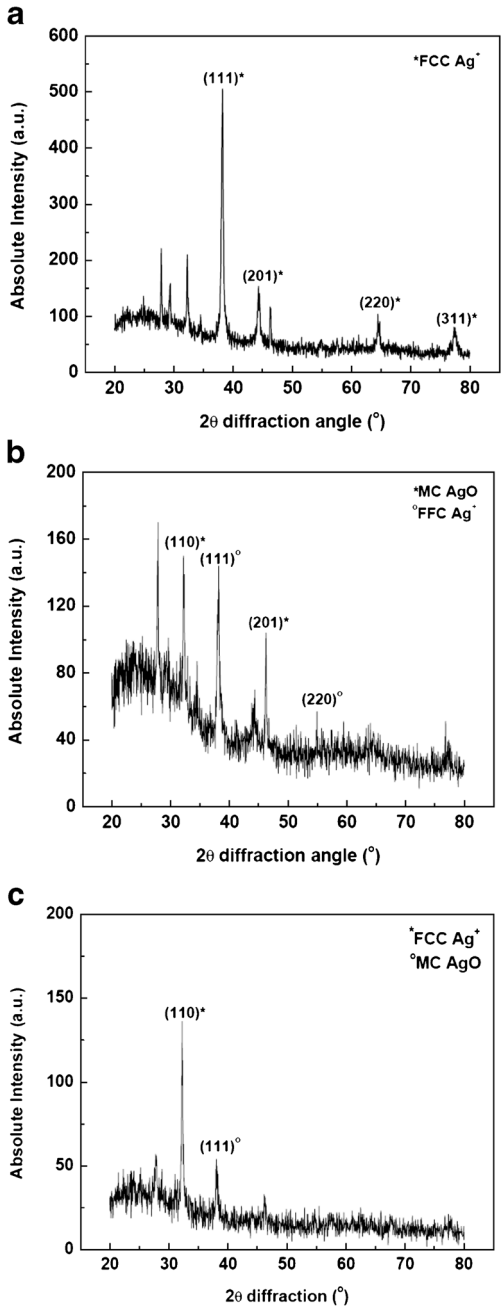

Fig. 4 Qualitative and quantitative analysis of AgNPs using X-ray diffraction spectroscopy: **a** DHM1-AgNPs showing peak of FCC crystals of AgNPs; **b** DHM2-AgNPs showing three peaks of FCC crystals and a peak of MC crystal of Ag_2O NPs; **c** PHM3-AgNPs major peak of FC crystals of Ag_2O and minor for Ag^+ NPs

Energy dispersive X-ray spectroscopy The EDS profile presented strong signal of Ag together with weak carbon (C), oxygen (O) and chlorine (Cl) peaks. The existence of C, O and Cl elements is inevitable due to the media ingredients which were used to grow algae as well as C and Cu grids used to analyse AgNPs. The EDS graph (Fig. S3a) obtained for DHM1-AgNPs exhibited presence of metallic Ag peaks with mass percentage of 76.2% and atomic percentage of 38.3%. Orbital energy for Ag revealed the presence of electrons in L-shell, and sub-shells α and indicated that sample was highly stable. DHM2-AgNPs showed presence of 66.8% Ag (Fig. S3b), while atomic percentage was 24.7%. Ag was present in Lα-shell of orbital mostly, and in β as well. PHM3-AgNP EDS graph illustrated percentage of Ag 60.7% by mass and 17.8% by atoms. Like other two species, Ag for this species was also indicated presence of Ag in L-shell of orbital largely with α sub-shell (Fig. S3c). The concentration of AgNPs according to Eqs. 1 and 2 in DHM1, DHM2 and PHM3-AgNPs were 2864.1, 3044.8 and 1716.5 nM, respectively.

Silver nanoparticles as therapeutics

Antibacterial activity Antibacterial activity of all three microalgae species was confirmed against 14 different strains of Gram-positive and Gram-negative bacteria (Fig. 5). PHM3-AgNPs with ovoid shape and larger size showed greater activity than DHM1-AgNPs and DHM2-AgNPs with sphere shape and smaller size. However, the ethanolic extract of all three species hardly showed any activity.

The study conducted here confirms zone of inhibition of 14 bacterial strains against DHM1-AgNPs, DHM2-AgNPs and PHM3-AgNPs. *Proteus mirabilis*, *A. junii*, *S. mutans*, *E. faecalis* and *S. dysenteriae* were strongly inhibited by DHM1-AgNPs (Fig. 5a). However, *S. typhi*, *Enterococcus* and *S. marcescens* showed were slightly inhibited whereas *S. aureus* and *P. aeruginosa* were not inhibited by all three algal species.

Antibacterial effects of DHM2-AgNPs (Fig. 5b) showed maximum activity on *P. mirabilis* and *Enterococcus*. DHM2-AgNPs inhibited growth of all other bacterial strains except for *S. aureus* and *P. aeruginosa*. Twelve strains were inhibited by PHM3-AgNPs (Fig. 5c) and with the maximum activity for *P. mirabilis*, *Enterococcus* and MRSA. Minimum inhibition was observed for *E. faecalis*, whereas *S. aureus* and *P. aeruginosa* were not inhibited.

Antifungal activity DHM1-AgNPs, DHM2-AgNPs and PHM3-AgNPs showed considerable zone of inhibition against *C. albicans*. Maximum inhibition was shown by PHM3-AgNPs, following DHM1-AgNPs (Fig. S4). A series of dilution from the stock solution (1 mg mL^{-1}) were made and tested, but maximum zone of inhibition was shown by the stock solution. The increased concentration did not show any significant change with baseline values at 1.75 mg mL^{-1}.

Cytotoxicity assay Synthesized AgNPs from three microalgae species were tested against HepG2, MCF7 and Huh7 cell lines. In vitro cytotoxicity against HepG2 (Fig. 6a) and MCF7 (Fig. 6b) was evaluated at different concentration in comparison with the standard drugs taxol and tamoxafin, respectively. A dose-dependent trend was

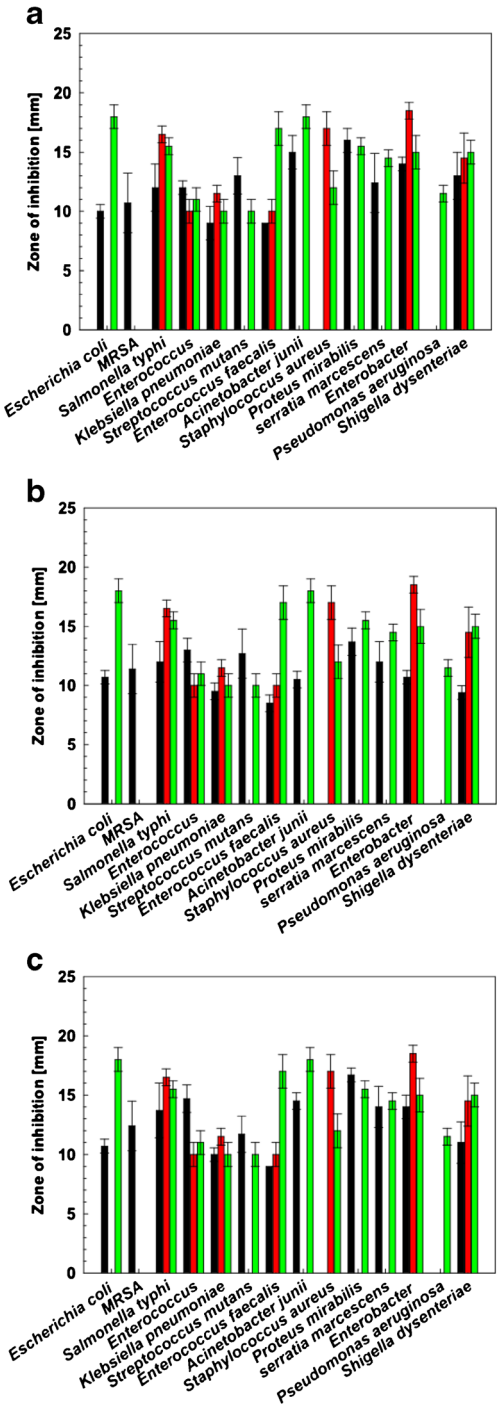

Fig. 5 Antibacterial activity of synthesized AgNPs. **a** DHM1-AgNPs, **b** DHM2-AgNPs and **c** PHM3-AgNPs (*black bar*) evaluated bacterial strains, (*red bar*) FEP and (*green bar*) TGC

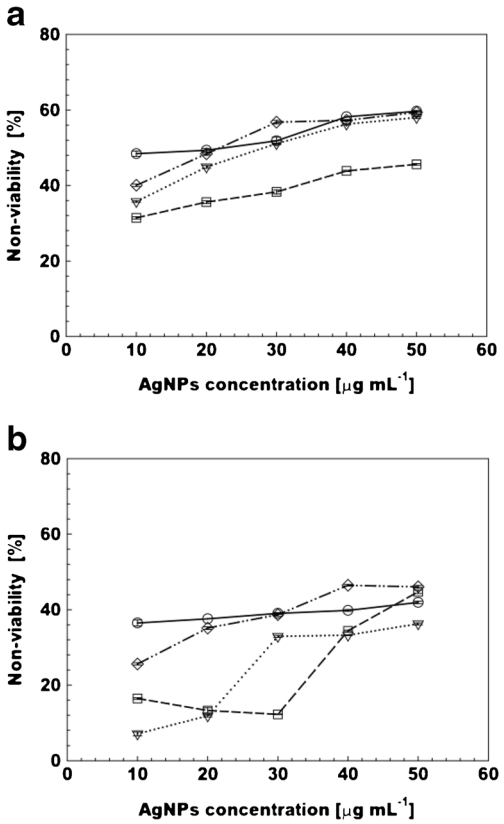

Fig. 6 Anticancer activity of synthesized AgNPs. **a** HepG2 tumour cell line and **b** MCF7 tumour cell line. (—○—) DHM1-AgNPs, (···▽··) DHM2-AgNPs, (–□–) PHM3-AgNPs and (·◇–) Taxol analysed with HepG2 and Temoxifin analysed with MCF7 line as control

observed for all three types of microalgae-mediated AgNPs. Activity of AgNPs against HepG2 was increased with increasing concentration. The calculated IC_{50} values for DHM1-AgNPs, DHM2-AgNPs were 0.30 and 0.289 μg mL^{-1}, respectively and the dose at these values was around 30 μg mL^{-1}. Taxol showed 46% cytotoxicity, which is less than the AgNPs of *Dictyospherium*. However, for PHM3-AgNPs, none of these dose ranges inhibited 50% of growth for cancerous cells. A proportional, dose-dependent and linearly increasing cytotoxic tendency against MCF7 was observed for DHM1-AgNPs, DHM2-AgNPs and IC_{50} values were 0.22 and 0.16 μg mL^{-1}, respectively. For PHM3-AgNPs, there was a decreasing trend and then an increasing dose-dependent trend was observed with an IC_{50} value of 0.16 μg mL^{-1}.

Apoptosis estimation assay (Fig. 7) with AgNP-treated cells exhibit a reduced amount of cells participating in G_0 to G_1 phase with an intensification at G_2 to M phase indicating cell cycle arrest at latter stages. HepG2 and MCF7 cells treated with AgNPs showed shearing of DNA and fragmentation providing a reason of cell death when treated.

Antiviral assay The $TCID_{50}$ ratio of viral suspension (Fig. 8) on Huh7 cells treated with AgNPs was used to gauge antiviral activity along with untreated infected cells as control. The DHM1-AgNPs showed maximum activity in a dose-dependent manner. DHM2-AgNPs and PHM3-AgNP exhibited a similar increase as the DHM1-AgNPs. At the same concentrations, the activity was highest for DHM1-AgNPs and least for PHM3-AgNPs.

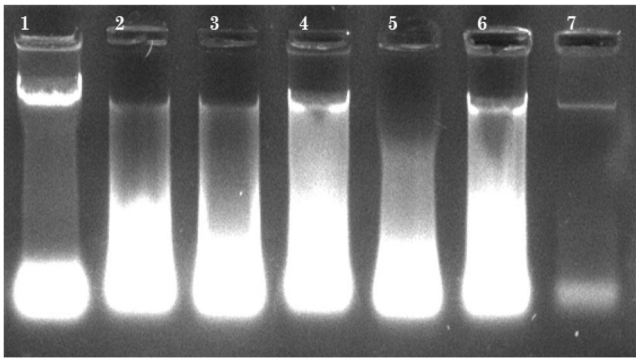

Fig. 7 DNA fragmentation analysis for apoptotic pathway assessment showing shearing and fragmentation of DNA bands in AgNP-treated cells, (*1*) PHM3-AgNPs at MCF7, (*2*) DHM1-AgNPs at MCF7, (*3*) DHM2-AgNPs at MCF7, (*4*) PHM3-AgNPs at HepG2, (*5*) DHM1-AgNPs at HepG2, (*6*) DHM2-AgNPs at HepG2, (*7*) control

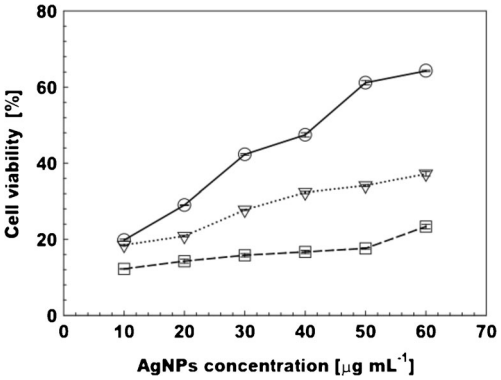

Fig. 8 Antiviral activity of AgNPs on NDV in Huh7 cell line. (—○—) DHM1-AgNPs, (···▽··) DHM2-AgNPs and (– –□– –) PHM3-AgNPs

Discussion

A series of various concentrations of silver nitrate ranging from 1 to 5 mM were used at different pH (data not shown) to ensure the maximum reduction of Ag^{+}, and results showed the peak at 5 mM. As the literature also showed that concentrations above this level could be toxic (Beer et al. 2012; Stensberg et al. 2011), the range was limited between 1 and 5 mM but intended to obtain optimum results. The reduction reaction resulting in the formation of algae-mediated AgNPs after UV spectrophotometric analysis showed that the SPR bands match with the findings of previous studies. AgNPs of marine microalgae species like *Chaetoceros calcitrans*, *C. salina*, *Isochrysis galbana* and *Tetraselmis gracilis* showed a peak at 420 nm (Merin et al. 2010). In another study (Kathiraven et al. 2015) on the marine alga *C. racemosa* at different time interval (3–24 h) showed a reduction in size and band shift from 440 to 413 nm. Therefore, SPR bands of our synthesized AgNPs lie in the same region and have closely related values (419, 421, 418 nm). The area under the peak indicates polydispersed and homogenized AgNPs.

Numerous studies showed different size ranges of AgNPs from different strains of algae, for instance, *Gelidiella acerosa* extracts exhibited spherical NPs of d_{av} 22 nm (Vivek et al. 2011), *Chlorococcum humicola* AgNPs presented d_{av} of 16 nm (Jena et al. 2013), whereas *Cystophora moniliformis* (Prasad et al. 2013) extract showed formation of AgNPs of 75 nm and beyond. Size and shape of NPs play characteristic role for specifying the properties of respective NPs. the reason for this phenomenon is the interaction between biocompounds such as proteins, polysaccharides, phenols, polyphenols and amines with metal ions determining the size and structure of NPs (Azizi et al. 2013).

TEM results obtained by our study correlates with TEM results generated by few other groups for algae mediated synthesis of metallic NPs which showed polydispersed NPs. *Sargassum longifolium* was used to manufacture gold NPs of 40–80 nm with spherical shape (Rajeshkumar et al. 2014) whereas AgNPs from *C. pyrenoidosa* were 2–20 nm spheres (Aziz et al. 2015). The polydispersed AgNPs attached to the biomolecules of algal cells consequently provide a size range due to different bond lengths. Smother edges of AgNPs could be due to protein or related molecules in the ethanol extract as described by Ahmad et al. (2010) for AgNP production from basil plant. Similarly, vibrational peaks observed in this study have closely related peaks as described by previous studies for algae-derived AgNPs from species such as *P. oedogonia* (Sinha et al. 2015) and *Chaetomorpha linum* (Kannan et al. 2013). These studies showed vibrational peaks for primary alcohol (3650–3200 cm^{-1}), alkanes (3300–2700 cm^{-1}) and aliphatic (1200–1000 cm^{-1}) compounds and are in accordance with our study. Appearance of primary alcohol indicates the strong reduction process involvement which allowed the synthesis of NPs. Alkanes and aldehydes suggest capping of AgNPs. However, almost every algal strain showed a unique characteristic peak. Previous studies also established the fact that carbonyl group from amino acid residues and proteins possess a stronger ability to bind metals. The process significance is to form a protective layer over the metallic NPs, prevention of agglomerates and stabilization of synthesized NPs (El-Rafie et al. 2013). Likewise, FTIR results suggested the successful formation of AgNPs for DHM1-AgNPs, DHM2-AgNPs and PHM3-AgNPs providing a confirmation of capping. In addition, all three FTIR analyses confirm the presence of both hydrophilic and hydrophobic functional groups attached to the AgNPs. The presence of reduced Ag is an indication of AgNP synthesis process completion as previous studies also revealed presence of pure metallic Ag (Jena et al. 2013). The shape of AgNPs plays an important role in cytotoxicity: predominant (111) face-centric cubic crystals always have greater antimicrobial activity due to smaller crystal size. However, monoclinic crystals (110) also have antimicrobial activity; in fact,

monoclinic crystal structure has synergistic effect with face-centric cubic structure and promotes antimicrobial activity. Recently, Raza et al. (2016) reported that even the triangular and larger spherical-shaped AgNPs show good antimicrobial activity.

Moreover, the variations in antimicrobial activities (results shown in Table S1) could be a consequence of morphological dissimilarity of bacterial strains. The physiology and genomics of bacterial strains play a major role with respect to the activity of AgNPs. In our previous study (Ashraf et al. 2014), we observed that the response of bacterial strains, even from the same species, was different for lysozyme-coated AgNPs. This difference in the antibacterial activity of AgNPs for different bacterial strains of the same species, even if there is no structural variation in the Ag nanoparticles may be due to the genome islands that are acquired through horizontal gene transfer (HGT). These genome islands are expected to possess some genes that may encode enzymes to resist the antimicrobial activity of AgNPs (Ashraf et al. 2014).

Numerous studies have been carried out to detect antibacterial activities if microalgae-mediated synthesized AgNPs. Inhibition of a bacterial strain depends on type of strain, type of AgNPs and microalgae species studied (Sudha et al. 2013). The results of this study showed different zone of inhibitions for diverse AgNPs when tested on various bacteria. Results also indicated activity towards both Gram-positive and Gram-negative bacteria. The AgNPs affect the morphology of *E. coli* and *S. aureus* as observed under TEM and SEM. The images displayed detached cell membrane from cell wall with appearance of electron-light region in the centre of bacterial cells (Feng et al. 2000). In the current study, EDS micrographs show different percentages of silver in the samples and the percentage of silver in the material can influence antimicrobial properties. Therefore, for quantitative analysis, the antimicrobial activities of these silver nanoparticles with the same Ag contents can be compared; however, organism-specific immune responses to different nanoparticle morphologies could lead to different observations. Similarly, microbial genomics could be another aspect that can influence antimicrobial properties of AgNPs as the microbes can acquire Ag-resistant genes through horizontal or lateral gene transfer and the effect of AgNPs was variable even if the percentage of silver was the same into these AgNPs (Ashraf et al. 2014). For qualitative analysis, silver percentage might not be a limiting factor in the antimicrobial properties of these AgNPs.

Fungal infections are strongly inhibited when exposed to Ag or AgNPs. *Sargassum longifolium*-mediated synthesized AgNPs have been used to inhibit several types of fungal strains (Rajeshkumar et al. 2014). Concentration plays an important role in drug activity. Ag^+ ions are effective at micromolar level, whereas AgNPs are effective at the nanomolar level, indicating a major difference between efficacy of Ag^+ and AgNPs and for effective cytotoxicity (Lok et al. 2006). Although previous studies on different tumour cell lines for algae-derived AgNPs showed positive results (Devi and Bhimba 2012; Roychoudhury et al. 2016; Vieira et al. 2016), our study showed similar activity even at low doses, probably due to the smaller size and better capping of the AgNPs. Cell apoptosis of cancer cell lines observed in our study opens another window to discuss how reactive oxygen species (ROS) may promote cell cycle propagation signalling entities. The ROS can also cause oxidative DNA damage (Alvarez-Gonzalez et al. 1999). DNA fragmentation is a feature of apoptosis as cell size reduces due to shrinkage (Gurunathan et al. 2013). The results clearly demonstrate the effect of size on the activity of AgNPs. This effect was predominantly observed in antiviral activity and in accordance to previous studies which concluded that size dependence is due to spatial restriction of binding of virions and AgNPs (Lu et al. 2008). Nevertheless, all three AgNPs of ethanolic extracts of microalgae expressed remarkable activity against NDV. The mechanism behind the antiviral activity of AgNPs is unknown. However, most likely the AgNPs directly bind with the virus glycoprotein envelope thus restricting virus penetration in host cells (Mori et al. 2013).

In conclusion, numerous studies have been done on the green synthesis of NPs using different biological resources such as prokaryotic and eukaryotic organisms. In the present study, a simple one-step methodology was adopted using green chemistry to synthesize AgNPs from ethanolic extracts of freshwater microalgae. Algal extracts of three species produced significant amount of versatile NPs when reacted with Ag. Microstructure characterization of biologically synthesized AgNPs was performed on SEM, TEM, XRD, FTIR and EDS. SEM and TEM showed homogeneous and uniformly distributed AgNPs with narrow size range for each species but of different sizes and shapes. XRD confirmed the crystalline structure of these AgNPs, as well as the formation of face-centred cubic and mono-centred structure of these AgNPs. FTIR indicated reduction and capping of Ag with different bio-compounds. Capping of carbonyls appeared to be responsible for the biosynthesis of AgNPs and their therapeutic activities. Antibacterial activity for a range of Gram-positive and negative bacteria, antifungal, anticancer and antiviral activities were observed. Lower concentration of effective dose can lead to minimum side effects almost eliminating the possibility of cytotoxicity for normal healthy cells. Antiviral activity with higher biocompatibility ratio can also be used as tool to counter viral infections.

Therefore, this study showed the efficiency of fresh water microalgae for the production of significant amount of

different size-range AgNPs with variable properties. However, investigation of bio-compounds involved in synthesis, reduction and capping of Ag still needs to be carried out.

Acknowledgements Authors are thankful to ASAB-NUST for the research and administrative facilities to conduct this research. Algae strains were collected and provided by Dr. Ehsan Ali fromUSPCAS-E, National University of Sciences and Technology (NUST), Islamabad, Pakistan. Anticancer and antiviral activity was conducted in supervision of Qaiser Mansoor from Institute of Biomedical and Genetic Engineering (IBGE). The authors are also thankful to SCME-NUST for providing the facility to analyse silver nanoparticles using various techniques such as XRD, SEM, EDS and FTIR etc. This research did not receive any specific grant from funding agencies in the public, commercial or not-for-profit sectors.

References

Abbasi E, Millani M, Fekri AS, Akbarzadeh A, Tayefi NH, Nikasa P, Joo SW, Hanifehpour Y, Nejati-Koshki K, Samiei M (2016) Silver nanoparticles: synthesis methods, bio-applications and properties. Crit Rev Microbiol 42:173–180

Ahmad N, Sharma S, Alam MK, Singh V, Shamsi S, Mehta B, Fatma A (2010) Rapid synthesis of silver nanoparticles using dried medicinal plant of basil. Colloid Surf B 81:81–86

Alvarez-Gonzalez R, Spring H, Müller M, Bürkle A (1999) Selective loss of poly (ADP-ribose) and the 85-kDa fragment of poly (ADP-ribose) polymerase in nucleoli during alkylation-induced apoptosis of HeLa cells. J Biol Chem 274:32122–32126

Asharani P, Wu YL, Gong Z, Valiyaveettil S (2008) Toxicity of silver nanoparticles in zebrafish models. Nanotechnology 19:255102

Ashraf S, Chatha MA, Ejaz W, Janjua HA, Hussain I (2014) Lysozyme-coated silver nanoparticles for differentiating bacterial strains on the basis of antibacterial activity. Nanoscale Res Lett 9(1):565. doi:10.1186/1556-276X-9-565

Aziz N, Faraz M, Pandey R, Shakir M, Fatma T, Varma A, Barman I, Prasad R (2015) Facile algae-derived route to biogenic silver nanoparticles: synthesis, antibacterial, and photocatalytic properties. Langmuir 31:11605–11612

Azizi S, Namvar F, Mahdavi M, Ahmad MB, Mohamad R (2013) Biosynthesis of silver nanoparticles using brown marine macroalga, *Sargassum muticum* aqueous extract. Materials 6:5942–5950

Beer C, Foldbjerg R, Hayashi Y, Sutherland DS, Autrup H (2012) Toxicity of silver nanoparticles—nanoparticle or silver ion? Toxicol Lett 208:286–292

Chomczynski P, Sacchi N (1987) Single-step method of RNA isolation by acid guanidinium thiocyanate-phenol-chloroform extraction. Anal Biochem 162:156–159

Devi JS, Bhimba BV (2012) Anticancer activity of silver nanoparticles synthesized by the seaweed *Ulva lactuca* in vitro. Sci Rep 1:242. doi:10.4172/scientific reports. 4242

Durán N, Marcato PD, Conti RD, Alves OL, Costa F, Brocchi M (2010) Potential use of silver nanoparticles on pathogenic bacteria, their toxicity and possible mechanisms of action. J Braz Chem Soc 21: 949–959

El Baky HHA, El-Baroty GS (2013) Healthy benefit of microalgal bioactive substances. J Aquat Sci 1:11–22

El-Rafie H, El-Rafie M, Zahran M (2013) Green synthesis of silver nanoparticles using polysaccharides extracted from marine macro algae. Carbohydr Polymer 96:403–410

Felsenstein J (1985) Confidence limits on phylogenies: an approach using the bootstrap. Evolution 39:783–791

Feng Q, Wu J, Chen G, Cui F, Kim T, Kim J (2000) A mechanistic study of the antibacterial effect of silver ions on *Escherichia coli* and *Staphylococcus aureus*. J. Biomed Mat Res 52:662–668

Feng X, Qi X, Li J, Yang LW, Qiu MC, Yin JJ, Lu F, Zhong JX (2011) Preparation, structure and photo-catalytic performances of hybrid Bi_2SiO_5 modified Si nanowire arrays. Appl Surf Sci 257:5571–5575

Freshney RI (2005) Culture of specific cell types. In: Culture of animal cells. Wiley Online Library

Gottesman R, Shukla S, Perkas N, Solovyov LA, Nitzan Y, Gedanken A (2010) Sonochemical coating of paper by microbiocidal silver nanoparticles. Langmuir 27:720–726

Gurunathan S, Kalishwaralal K, Vaidyanathan R, Deepak V, Pandian SRK, Muniyandi JH, Hariharan H, Eom SH (2009) Biosynthesis, purification and characterization of silver nanoparticles using *Escherichia coli*. Colloid Surf B 74:328–335

Gurunathan S, Han JW, Eppakayala V, Jeyaraj M, Kim J-H (2013) Cytotoxicity of biologically synthesized silver nanoparticles in MDA-MB-231 human breast cancer cells. Biomed Res Int 2013: 535796

Haaf F, Sanner A, Straub F (1985) Polymers of N-vinylpyrrolidone: synthesis, characterization and uses. Polym J 17:143–152

Hall TA (1999) BioEdit: a user-friendly biological sequence alignment editor and analysis program for Windows 95/98/NT. Nucl Acids Symp Ser 41:95–98

Ihsan M, Niaz A, Rahim A, Zaman MI, Arain MB, Sharif T, Najeeb M (2015) Biologically synthesized silver nanoparticle-based colorimetric sensor for the selective detection of Zn^{2+}. RSC Adv 5: 91158–91165

Ishtiaq S, Ashraf M, Hayat MQ, Asrar M (2013) Phytochemical analysis of *Nigella sativa* and its antibacterial activity against clinical isolates identified by ribotyping. Int J Agric Biol 15:1151–1156

Jena J, Pradhan N, Dash B, Sukla L, Panda P (2013) Biosynthesis and characterization of silver nanoparticles using microalga *Chlorococcum humicola* and its antibacterial activity. Int J Nanomater Biostruct 3:1–8

Joana Gil-Chávez G, Villa JA, Fernando Ayala-Zavala J, Basilio Heredia J, Sepulveda D, Yahia EM, González-Aguilar GA (2013) Technologies for extraction and production of bioactive compounds to be used as nutraceuticals and food ingredients: an overview. Comp Rev Food Sci Food Saf 12:5–23

Kannan RRR, Arumugam R, Ramya D, Manivannan K, Anantharaman P (2013) Green synthesis of silver nanoparticles using marine macroalga *Chaetomorpha linum*. Appl Nanosci 3:229–233

Karcioglu L, Tanis H, Comlekcioglu N, Diraz E, Kirecci E, Aygan A (2011) Antimicrobial activity of *Salvia trichoclada* in southern Turkey. Int J Agric Biol 13:134–136

Kathiraven T, Sundaramanickam A, Shanmugam N, Balasubramanian T (2015) Green synthesis of silver nanoparticles using marine algae *Caulerpa racemosa* and their antibacterial activity against some human pathogens. Appl Nanosci 5:499–504

Liu X, Atwater M, Wang J, Huo Q (2007) Extinction coefficient of gold nanoparticles with different sizes and different capping ligands. Colloid Surf B 58:3–7

Lok CN, Ho CM, Chen R, He QY, Yu WY, Sun H, Tam PK, Chiu JF, Che CM (2006) Proteomic analysis of the mode of antibacterial action of silver nanoparticles. J Proteome Res 5:916–924

Lu L, Sun RW, Chen R, Hui CK, Ho CM, Luk JM, Lau GK, Che CM (2008) Silver nanoparticles inhibit hepatitis B virus replication. Antiviral Ther 13:253

Mahdavi M, Ahmad MB, Haron MJ, Namvar F, Nadi B, Rahman MZA, Amin J (2013) Synthesis, surface modification and characterisation of biocompatible magnetic iron oxide nanoparticles for biomedical applications. Molecules 18:7533–7548

Marcos-Zambrano LJ, Escribano P, Sánchez C, Muñoz P, Bouza E, Guinea J (2014) Antifungal resistance to fluconazole and echinocandins is not emerging in yeast isolates causing fungemia

in a Spanish tertiary care center. Antimicrob Agents Chemother 58: 4565–4572

Martínez-Gutierrez F, Thi EP, Silverman JM, de Oliveira CC, Svensson SL, Vanden Hoek A, Sanchez EM, Reiner NE, Gaynor EC, Pryzdial EL, Conway EM (2012) Antibacterial activity, inflammatory response, coagulation and cytotoxicity effects of silver nanoparticles. Nanomedicine 8:328–336

Merin DD, Prakash S, Bhimba BV (2010) Antibacterial screening of silver nanoparticles synthesized by marine micro algae. Asian Pac J Trop Med 3:797–799

Mermel LA, Allon M, Bouze E, Craven DE, Flynn P, Grady NPO, Raad II, Rajinder BJA, Sheretz RJ, Warren DK (2009) Clinical practice guidelines for the diagnosis and management of intravascular catheter-related infection: 2009 update by the Infectious Diseases Society of America. Clin Infect Dis 49:1–45

Mohamed S, Hashim SN, Rahman HA (2012) Seaweeds: a sustainable functional food for complementary and alternative therapy. Trend Food Sci Technol 23:83–96

Mori Y, Ono T, Miyahira Y, Nguyen VQ, Matsui T, Ishihara M (2013) Antiviral activity of silver nanoparticle/chitosan composites against H1N1 influenza a virus. Nanoscale Res Lett 8:1–6

Mukherjee P, Ahmad A, Mandal D, Senapati S, Sainkar SR, Khan MA, Parishcha R, Ajaykumar PV, Alam M, Kumar R, Sastry M (2001) Fungus-mediated synthesis of silver nanoparticles and their immobilization in the mycelial matrix: a novel biological approach to nanoparticle synthesis. Nano Lett 1:515–519

Namasivayam S, Jayakumar D, Kumar VR, Bharani R (2015) Antibacterial and anticancerous biocompatible silver nanoparticles synthesised from the cold tolerant strain of *Spirulina platensis*. J Coast Life Sci 3:265–272

Namvar F, Mohamed S, Fard SG, Behravan J, Mustapha NM, Alitheen NBM, Othman F (2012) Polyphenol-rich seaweed (*Eucheuma cottonii*) extract suppresses breast tumour via hormone modulation and apoptosis induction. Food Chem 130:376–382

Nayak RR, Pradhan N, Behera D, Pradhan KM, Mishra S, Sukla LB, Mishra BK (2011) Green synthesis of silver nanoparticle by *Penicillium purpurogenum* NPMF: the process and optimization. J Nanopart Res 13:3129–3137

Nishino T, Fukuda A, Nagumo T, Fujihara M, Kaji E (1999) Inhibition of the generation of thrombin and factor Xa by a fucoidan from the brown seaweed *Ecklonia kurome*. Thrombosis Res 96:37–49

Patel V, Berthold D, Puranik P, Gantar M (2015) Screening of cyanobacteria and microalgae for their ability to synthesize silver nanoparticles with antibacterial activity. Biotechnol Rep 5:112–119

Pizzi M (1950) Sampling variation of the fifty per cent end-point, determined by the reed-Muench (Behrens) method. Human Biol 22:151–190

Prasad TN, Kambala VSR, Naidu R (2013) Phyconanotechnology: synthesis of silver nanoparticles using brown marine algae *Cystophora moniliformis* and their characterisation. J Appl Phycol 25:177–182

Rajeshkumar S, Malarkodi C, Paulkumar K, Vanaja M, Gnanajobitha G, Annadurai G (2014) Algae mediated green fabrication of silver nanoparticles and examination of its antifungal activity against clinical pathogens. Int J Metals 2014:692643

Raza MA, Kanwal Z, Rauf A, Sabri AN, Riaz S, Naseem S (2016) Size- and shape-dependent antibacterial studies of silver nanoparticles synthesized by wet chemical routes. Nanomaterials 6(4):74. doi: 10.3390/nano6040074

Rogers SO, Bendich AJ (1994) Extraction of total cellular DNA from plants, algae and fungi. In: Gelvin SB, Schilperoort (eds) Plant molecular biology manual section D. Kluwer, Dordrecht, pp 183–190

Roychoudhury P, Gopal PK, Paul S, Pal R (2016) Cyanobacteria assisted biosynthesis of silver nanoparticles—a potential antileukemic agent. J Appl Phycol 28:3387–3394

Satapathy S, Shukla SP, Sandeep KP, Singh AR, Sharma N (2015) Evaluation of the performance of an algal bioreactor for silver nanoparticle production. J Appl Phycol 27:285–291

Sharma A, Sharma S, Sharma K, Chetri SPK, Vashishtha A, Singh P, Kumar R, Rathi B, Agrawal V (2016) Algae as crucial organisms in advancing nanotechnology: a systematic review. J Appl Phycol 28:1759–1774

Sinha SN, Paul D, Halder N, Sengupta D, Patra SK (2015) Green synthesis of silver nanoparticles using fresh water green alga *Pithophora oedogonia* (Mont.) Wittrock and evaluation of their antibacterial activity. Appl Nanosci 5:703–709

Stein JR (1979) Handbook of phycological methods: culture methods and growth measurements, vol 1. Cambridge University Press, Cambridge

Stensberg MC, Wei Q, McLamore ES, Porterfield DM, Wei A, Sepúlveda MS (2011) Toxicological studies on silver nanoparticles: challenges and opportunities in assessment, monitoring and imaging. Nanomedicine 6:879–898

Sudha S, Rajamanickam K, Rengaramanujam J (2013) Microalgae mediated synthesis of silver nanoparticles and their antibacterial activity against pathogenic bacteria. Indian J Exp Biol 51:393–399

Sunitha S, Rao A, Abraham L, Dhayalan E, Thirugnanasambandam R, Ganesh Kumar V (2015) Enhanced bactericidal effect of silver nanoparticles synthesized using marine brown macroalgae. J Chem Pharma Res 7:191–195

Tamura K, Stecher G, Peterson D, Filipski A, Kumar S (2013) MEGA 6: molecular evolutionary genetics analysis version 6.0. Mol Biol Evol 30:2725–2729

Thompson JD, Gibson TJ, Plewniak F, Jeanmougin F, Higgins DG (1997) The CLUSTAL X windows interface: flexible strategies for multiple sequence alignment aided by quality analysis tools. Nucleic Acids Res 25:4876–4882

Vieira AP, Stein EM, Andreguetti DX, Colepicolo P, da Costa Ferreira AM (2016) Preparation of silver nanoparticles using aqueous extracts of the red algae *Laurencia aldingensis* and *Laurenciella* sp. and their cytotoxic activities. J Appl Phycol 28:2615–2622

Vivek M, Kumar PS, Steffi S, Sudha S (2011) Biogenic silver nanoparticles by *Gelidiella acerosa* extract and their antifungal effects. Avicenna J Med Biotechnol 3:143–148

You C, Han C, Wang X, Zheng Y, Li Q, Hu X, Sun H (2012) The progress of silver nanoparticles in the antibacterial mechanism, clinical application and cytotoxicity. Mol Biol Rep 39:9193–9201